



Chinese Pharmaceutical Association
Institute of Materia Medica, Chinese Academy of Medical Sciences

Acta Pharmaceutica Sinica B

www.elsevier.com/locate/apsb
www.sciencedirect.com



ORIGINAL ARTICLE

Development of LAG-3/FGL1 blocking peptide and combination with radiotherapy for cancer immunotherapy



Yuzhen Qian^{a,†}, Yixuan Sun^{b,†}, Peishang Shi^a, Xiuman Zhou^b,
Qiongqiong Zhang^a, Qingyu Dong^b, Shengzhe Jin^a, Lu Qiu^{a,b},
Xiaoshuang Niu^b, Xiaowen Zhou^a, Wenshan Zhao^a, Yahong Wu^{a,c},
Wenjie Zhai^{a,c,*}, Yanfeng Gao^{a,b,*}

^aSchool of Life Sciences, Zhengzhou University, Zhengzhou 450001, China

^bSchool of Pharmaceutical Sciences (Shenzhen), Shenzhen Campus of Sun Yat-sen University, Shenzhen 518107, China

^cInternational Joint Laboratory for Protein and Peptide Drugs of Henan Province, Zhengzhou University, Zhengzhou 450001, China

Received 24 September 2023; received in revised form 20 November 2023; accepted 23 November 2023

KEY WORDS

LAG-3;
FGL1;
PD-1;
PD-L1;
Peptide;
Immune checkpoint;
Radiotherapy;
Cancer immunotherapy

Abstract Aside from antibodies, peptides show great potential as immune checkpoint inhibitors (ICIs) due to several advantages, such as better tumor penetration and lower cost. Lymphocyte-activation gene 3 (LAG-3) is an immune checkpoint which can induce T cell dysfunction through interaction with its soluble ligand fibrinogen like protein-1 (FGL1). Here, we found that LAG-3 expression was higher than programmed cell death protein 1 (PD-1) in multiple human cancers by TCGA databases, and successfully identified a LAG-3 binding peptide LFP-6 by phage display bio-panning, which specifically blocks the interaction of LAG-3/FGL1 but not LAG-3/MHC-II. Subsequently, D-amino acids were introduced to substitute the N- and C-terminus of LFP-6 to obtain the proteolysis-resistant peptide LFP-D1, which restores T cell function *in vitro* and inhibits tumor growth *in vivo*. Further, a bispecific peptide LFOP targeting both PD-1/PD-L1 and LAG-3/FGL1 was designed by conjugating LFP-D1 with PD-1/PD-L1 blocking peptide OPBP-1(8–12), which activates T cell with enhanced proliferation and IFN- γ production. More importantly, LFOP combined with radiotherapy significantly improve the T cell

*Corresponding authors.

E-mail addresses: wjzhai@zzu.edu.cn (Wenjie Zhai), gaoyf29@mail.sysu.edu.cn (Yanfeng Gao).

[†]These authors made equal contributions to this work.

Peer review under the responsibility of Chinese Pharmaceutical Association and Institute of Materia Medica, Chinese Academy of Medical Sciences.

<https://doi.org/10.1016/j.apsb.2023.12.011>

2211-3835 © 2024 The Authors. Published by Elsevier B.V. on behalf of Chinese Pharmaceutical Association and Institute of Materia Medica, Chinese Academy of Medical Sciences. This is an open access article under the CC BY-NC-ND license (<http://creativecommons.org/licenses/by-nc-nd/4.0/>).

infiltration in tumor and elevate systemic antitumor immune response. In conclusion, we developed a novel peptide blocking LAG-3/FGL1 which can restore T cell function, and the bispecific peptide synergizes with radiotherapy to further enhance the antitumor immune response.

© 2024 The Authors. Published by Elsevier B.V. on behalf of Chinese Pharmaceutical Association and Institute of Materia Medica, Chinese Academy of Medical Sciences. This is an open access article under the CC BY-NC-ND license (<http://creativecommons.org/licenses/by-nc-nd/4.0/>).

1. Introduction

Immune checkpoint blockade is a revolutionized treatment strategy for diverse cancers to improve the outcomes of patients¹. Blocking the interaction of PD-1/PD-L1 can alleviate the dysfunctional T cell as well significantly increase therapeutic efficacy of adjuvant radiotherapy and chemoradiotherapy^{2,3}. Despite several antibodies blocking PD-1/PD-L1 pathway were approved by U.S. Food and Drug Administration (FDA)⁴, limited response rates and immune-related adverse events have also been observed in patients^{5,6}. Consequently, attention has been increasingly focused on targeting alternative immune checkpoints such as LAG-3⁷, T cell immunoglobulin domain and mucin domain-3⁸ and T cell immunoreceptor with Ig and ITIM domains^{9,10}.

Among these immune checkpoints, LAG-3 expresses on a host of immune cell subtypes as a co-inhibitory receptor, including activated T cells¹¹, natural killer (NK) cells, dendritic cells (DCs)¹², monocytes and B cells. LAG-3 has the homologous domain architectures with CD4 protein¹³, containing four extracellular Ig domains (D1–D4) including an approximate extra 30-amino-acid loop in D1 domain¹⁴. The D1 domain of LAG-3 interacts with the shared ligand major histocompatibility complex class II (MHC-II) but confers higher affinity than that of CD4¹⁵. LAG-3 negatively regulates T cell expansion and controls the size of the memory T cell pool¹⁶. Recently, FGL1 was reported as a major functional ligand of LAG-3 independent from MHC-II by attenuation of T cell activation, proliferation and cytokine production¹⁷.

FGL1, a member of the fibrinogen family protein, is secreted from hepatocytes and contributes to liver damage repair^{18,19}, glucose and lipid metabolism²⁰, and immune homeostasis^{21,22} under physiological conditions, but overexpresses in tumor cells and induces the immunosuppression by engaging with LAG-3. High levels of FGL1 are strongly associated with high densities of LAG-3⁺ cells and negative association with CD8⁺ T cells in hepatocellular carcinoma tissues compared to adjacent normal liver tissues²³. Multiple studies have emphasized the potential of targeting LAG-3/FGL1 as the next generation of immune checkpoint therapy²⁴. Recombinant FGL1 protein partially inhibited antigen-specific T cell activation in an LAG-3 dependent fashion, and antibody blockade or silencing LAG-3/FGL1 can skew T cell immunosuppression in the tumor microenvironment and further inhibit tumor growth *in vivo*¹⁷. Therefore, the novel immune checkpoint LAG-3/FGL1 is an immunosuppressive pathway non-redundant to PD-1/PD-L1, which could be an ideal target for cancer immunotherapy.

The intimate relationship between the co-expression and synergistic inhibitory effect of the LAG-3 and PD-1 in tumor infiltrating lymphocytes (TILs) support the investigation on co-blockade antibodies²⁵. The synergistic effect of LAG-3/FGL1 blockade in combination with anti-PD-1 therapy has been

confirmed in animal models²⁶. More importantly, higher plasma FGL1 levels were significantly correlated with a worse therapeutic response to anti-PD-1/PD-L1 therapy in non-small cell lung carcinoma and melanoma patients, which indicated the potential biomarker role of FGL1 to predict the outcome of PD-1/PD-L1 blockade treatment¹⁷. Wan et al.²⁷ designed a new nanoparticle loading FGL1 siRNA (siFGL1) and PD-L1 siRNA (siPD-L1) which can significantly reduce the protein levels of FGL1 and PD-L1, and increase the infiltration of effector CD4⁺ and CD8⁺ T cells in Lewis lung cancer model. The potential of combination of PD-L1 signaling blockade and *FGL1* gene silencing in pH-responsive hybrid membrane-coated nanoparticles also exhibited high synergistic therapeutic efficacy against breast cancer *in vitro* and *in vivo*²⁸. All these findings strongly support the promising and powerful therapeutic strategy of dual blockade of LAG-3/FGL1 and PD-1/PD-L1 pathways.

In contrast to therapeutic antibodies, peptides have lower immunogenicity, better tumor penetration, as well as easier synthesis and modification with lower cost²⁹. Up to now, peptides targeting PD-1/PD-L1³⁰, TIGIT/PVR³¹, and CD47/Sirpα³², have been developed to achieve great antitumor effects through harnessing the immune response mediated by CD8⁺ T cells or macrophages^{33,34}. In our previous study, we identified a cyclic peptide C25, which could block the interaction of LAG-3/MHC-II and inhibit tumor growth in CT26 and B16 tumor models³⁵, but whether it could block LAG-3/FGL1 remains unclear. Recently, we also designed a dual targeting peptide which conjugated the minimal active fragment of PD-1/PD-L1 blocking peptide OPBP-1³⁶ with peptide inhibitor ^DA7R targeting vascular endothelial growth factor pathway, which can elicit synergistic antitumor effects³⁷. However, there are no peptide inhibitors reported to specifically block LAG-3/FGL1, not to mention bispecific peptide inhibitors targeting both LAG-3/FGL1 and PD-1/PD-L1.

Radiotherapy (RT) can increase the rate of tumor cell death to release tumor antigens, thus to trigger DC maturation and promote T cell activation and migration³⁸. Otherwise, RT also mobilizes the immunosuppressive cells, such as Treg cells, M2 macrophages and myeloid suppressive cells (MDSCs), as well increases the expression of inhibitory immune checkpoints, such as PD-1 and LAG-3³⁹, which enables tumor cells to evade the immune surveillance and greatly decreases the RT treatment efficacy. Previous studies have demonstrated that the combination of PD-1/PD-L1 blockade with radiotherapy yielded excellent tumor inhibition both in primary and secondary tumors^{40,41}. It has been investigated that FGL1 expression in tissues including plasma, liver⁴², lung⁴³ and gastric⁴⁴ increased after radiation exposure, suggesting that plasma FGL1 showed positive correlation with radiation doses. Hence, we envisaged that radiotherapy increased FGL1 expression in tumor cell and combined it with blockade LAG-3 and PD-1 would synergistically enhance the efficacy of cancer immunotherapy.

In the present study, we screened LAG-3 binding peptides by phage display bio-panning and modified the candidate peptide LFP-6 by D-amino acid substitution to get the hydrolysis-resistant peptide LFP-D1. The binding affinity, LAG-3/FGL1 blocking activity and T cell activation efficacy were determined. Subsequently, a bispecific peptide LFOP was designed by conjugation of PD-1/PD-L1 blocking peptide OPBP-1(8–12) with LFP-D1. The *in vitro* bioactivity of peptide LFOP and the antitumor activity was determined combination with radiotherapy or alone. Our study proposed a novel strategy to design immune checkpoint peptide inhibitors and amplify antitumor immune response through combination treatment.

2. Materials and methods

2.1. Cell lines and reagents

CHO-K1 and Jurkat leukemia T cells overexpressing hLAG-3 were established by lentiviral transfection and selected with 1 mg/mL puromycin. They were cultured in RPMI-1640 medium (Gibco, Grand Island, USA) containing 10% heat-inactivated FBS (BI, USA), 100 U/mL penicillin and 100 µg/mL streptomycin (Solarbio, China) in 37 °C and 5% CO₂ incubator. Human peripheral blood mononuclear cells (PBMCs) from healthy donors were diluted with PBS (pH 7.2) and separated with Ficoll density gradient and centrifuge (2000 rpm, 30 min, 25 °C) (Thermo Fisher Scientific, Heraeus Multifuge X1R, USA)⁴⁵. The isolated cells were resuspended at 1 × 10⁶ cells/mL in complete RPMI-1640 medium. To isolate the mouse spleen lymphocytes, the mouse spleen was extracted and digested into single cells by collagenase IV (17104-019, Gibco) and DNase I (Sigma, USA). We adjusted the cells density into 2 × 10⁶ cells/mL and cultured in complete RPMI-1640 medium. The HepG2 cells and MC38 cells were cultured in complete DMEM (Gibco, Grand Island, USA) medium.

The antibodies used for flow cytometry (BD FACS Celesta, USA) are listed in Supporting Information Table S1. And proteins used for MST and blocking assay are listed in Supporting Information Table S2.

2.2. Subtractive phage bio-panning

Ph.D.-7 peptide library (New England BioLabs) was used for peptide screening. 1 × 10⁶ CHO-K1 cells and CHO-K1-hLAG-3 cells were harvested and washed by serum-free medium and blocked with 200 µL bovine serum albumin (5 mg/mL, BSA, Sigma) for 1 h at 4 °C. Then, Ph.D.-7 peptide library aliquot containing 1 × 10¹¹ phages were added to CHO-K1 cells and incubated at 37 °C for 1 h. Later, the supernatant was incubated with CHO-K1-hLAG-3 cells at 37 °C for 2 h. Next, the phage solution was removed, and the CHO-K1-hLAG-3 cells was washed with PBST (pH 5.0) for 5 times and PBST (pH 7.4) for 2 times to remove the unbound phages. The cells were spitted with sterile water and the bound phages were eluted with 200 mmol/L Glycine–HCl (pH 2.2) for 20 min at room temperature. The solution was neutralized with 1 mol/L Tris–HCl (pH 9.1) according to the instructions. 10 µL sample was taken from the eluate for titrating, and the rest was used for amplification by *E. coli* ER2738. The screening procedure was repeated for 5 times with increased incubation time and the concentration of Tween-20.

Individual clones were randomly picked for detecting the nucleotide sequences by Sangon Biotech after the fifth-round panning.

2.3. MST

The affinity of candidate peptides to LAG-3, FGL1 or PD-L1 were tested by microscale thermophoresis (MST) (NanoTemper Technologies GmH, Germany). Human LAG-3-His protein, mouse LAG-3-His protein, human FGL1-His protein, mouse FGL1-His protein, human PD-L1-His protein and mouse PD-L1-His protein were labeled by RED-tris-NTA 2nd Generation dye (MO-L018, Nano Temper Technologies GmH, Germany). LFP-6, LFP-D1 and LFOP peptides were diluted into gradient concentrations with PBST (0.05% Tween-20). The equal volumes of LAG-3-His, FGL1-His or PD-L1-His protein solution labeled with dye were mixed with the gradient concentrations of peptides solution at room temperature for 5 min following the MST assay protocol. Then, the mixture was loaded onto capillary for further detection of the dissociation constant (K_D) values, which were calculated by the Nano Temper analysis software MO. Affinity Analysis.

2.4. Induction of HLA-DR expression on THP-1 cells

The expression of HLA-DR on THP-1 cells was upregulated with the stimulation of recombinant human IFN- γ ³⁵. 4 × 10⁵ cells/mL THP-1 cells were cultured in RPMI-1640 medium containing 10% FBS with 80 ng/mL of rhIFN- γ for 36 h. Then, the HLA-DR expression level was analyzed by flow cytometry with anti-human HLA-DR PerCP-Cy5.5.

2.5. Blocking assays

For blocking the interaction of LAG-3/FGL1, we incubated CHO-K1-hLAG-3 or CHO-K1-mLAG-3 cells with candidate peptides at different concentrations for 30 min at 4 °C. The mixture was added with recombinant human FGL1-Fc protein or mouse FGL1-Fc protein for 30 min at 4 °C, followed by incubation with the PE-conjugated goat anti-human IgG1 antibodies (anti-Fc-PE). The mixture without peptide was used as a positive control, and the one in which cells only incubated with the anti-Fc-PE antibody served as a negative control. The blocking efficacy (%) was calculated according to Eq. (1):

$$\text{The blocking efficacy (\%)} = \frac{\text{MFI of the positive control} - \text{MFI of the tested peptides}}{\text{MFI of the positive control}} \times 100 \quad (1)$$

The IC₅₀ was determined from dose response curves illustrated by GraphPad Prism.

For blocking the interaction of LAG-3/MHC-II, we incubated LAG-3-Fc protein with peptide solution for 30 min, and the mixture was added into THP-1 cells expressing HLA-DR to incubate for 30 min and anti-Fc-PE antibody was added at last.

For blocking the interaction of CD4/MHC-II, the recombinant human CD4-His & Fc protein was incubated with dissolved peptide solution. The remained steps were similar to those described above.

For blocking the interaction of PD-1/PD-L1, the blocking assays were performed as previously reported³⁷.

2.6. In vitro proteolysis stability assay

Proteolysis resistance properties of LFP-6 and LFP-D1 peptide were detected using RP-HPLC (Waters 2695, Waters, USA). For incubating with human serum, LFP-6 and LFP-D1 were dissolved in normal saline and diluted with 10% human serum to the concentration of 0.5 mmol/L, and incubated in a metal bath at 37 °C. For incubating with MC38 cells, LFP-6 and LFP-D1 were dissolved in normal saline and incubated with MC38 cells for 48 h in 37 °C and 5% CO₂ incubator. 200 µL of each solution was sampled at various time intervals from 0 to 48 h, and immediately mixed with 100 µL 10% HClO₄ solution followed by centrifugation at 15,000 rpm for 15 min twice. The samples were analyzed by RP-HPLC.

2.7. PBMCs activating assay

PBMCs from healthy donors were separated by Ficoll density gradient solution and centrifugation. The isolated mononuclear cells (2×10^5 cells/well) were treated with 1 µg/mL human anti-CD3 (OKT3, Biogems) and 1 µg/mL human anti-CD28 (CD28.2, Biogems) stimulatory antibodies in 48 well plates. 100 µmol/L LFP-D1 or C25 peptides were respectively added to the system and cocultured for 72 h. The Giogiplug protein transport inhibitors (51-2301KZ, BD GolgiPlug) were added in the last 4 h. To assess the ability of LFP-D1 and C25 on activating T cell, we analyzed the secretion of IFN- γ by flow cytometry after fixing and permeabilizing the collected cells.

2.8. Cell proliferation

In order to detect the effects of LFP-D1 or LFOP peptide on the proliferation of MC38 cells, we seeded MC38 cells (5000 cells/well) into 24 well plates and incubated with PBS (pH 7.2), LFP-D1 (100 µmol/L) or LFOP (100 µmol/L) for 7 days, and counted the numbers of cells daily. For MTT assay, we seeded MC38 cells (4000 cells/well) into 96 well plates and incubated with PBS (pH 7.2), LFP-D1 (100 µmol/L) or LFOP (100 µmol/L) for 24, 48 and 72 h. The MTT reagent (M2003, Sigma, USA) was added into the system to determine the absorbance at 490 nm by SpectraMax iD5 (Molecular Devices, USA).

2.9. Colony formation

In order to detect the effects of LFP-D1 or LFOP peptide on the colony formation of MC38 cells. We seeded MC38 cells (800 cells/well) into 6 well plates and incubated with PBS (pH 7.2), LFP-D1 (100 µmol/L) or LFOP (100 µmol/L) for 10 days. Next, cells were fixed with 4% polyformaldehyde for 30 min. Finally, 0.2% crystal violet was used to stain the cells.

2.10. Real-time quantitative reverse transcription PCR (qRT-PCR)

The qRT-PCR assay was performed to detect the expression of *Fgl1* and *Pd-11*. RNA was extracted from HepG2 cells, HT29 cells, SW620 cells, SW480 cells and MC38 cells and the first-strand cDNA was synthesized. The PCR reaction was conducted with LightCycler 480 SYBR Green I Master (Roche, 04707516001, Switzerland). The primer sequences of the human *FGL1*, mouse *Fgl1*, mouse *Pd-11*, human *GAPDH* and mouse β -actin are listed in Supporting Information Table S3.

2.11. Coculture assay

For the coculture of Jurkat-hLAG-3 and HepG2 cells or SW620 cells, we treated Jurkat-hLAG-3 cells (2×10^5 cells/well) with 1 µg/mL human anti-CD3 and 1 µg/mL human anti-CD28 stimulatory antibodies, and cocultured with HepG2 cells or SW620 cells (1×10^5 cells/well) in 24 well plates, with or without LFP-D1 (100 µmol/L) for 48 h. The Giogiplug protein transport inhibitor was added at last 4 h. Next, we tested the secretion level of IL-2 from Jurkat-hLAG-3 cells by staining with anti-human CD45 FITC and anti-human IL-2 APC after fixation and permeabilization.

For the coculture of PBMCs and HepG2 cells assay, the PBMCs were labeled with CFSE (0.5 µmol/L), and treated with 1 µg/mL human anti-CD3 and 1 µg/mL human anti-CD28 stimulatory antibodies. The stimulated PBMCs (2×10^5 cells/well) were cocultured with HepG2 cells (2×10^4 cells/well) for 3 days with or without 100 µmol/L tested peptides [LFP-D1, OPBP-1(8–12), LFP-D1 plus OPBP-1(8–12) or LFOP], and then Giogiplug protein-transport inhibitor was added at the last 4 h. Next, we determined the proliferation of CD8⁺ and CD4⁺ T cells as well the secretion of IFN- γ by flow cytometry.

For the coculture of mouse splenocytes and MC38 cells assay, we extracted the spleen from MC38 tumor-bearing mice and lysed it with $1 \times$ ACK lysis buffer. Next, the lymphocytes were treated with 1 µg/mL mouse anti-CD3 (17A2, Biogems) and 1 µg/mL mouse anti-CD28 (37.51, Biogems) stimulatory antibodies, and cocultured with MC38 cells for 3 days with or without 100 µmol/L tested peptides [LFP-D1, OPBP-1(8–12), LFP-D1 plus OPBP-1(8–12) or LFOP]. We also tested the proliferation and IFN- γ secretion of CD8⁺ and CD4⁺ T cells by flow cytometry.

2.12. Tumor models and treatments

For LFP-D1 treatment, we subcutaneously injected 1×10^6 MC38 cells into the right flank of six-week-old female C57BL/6 mice. 1 or 3 mg/kg LFP-D1 were administered every day when the tumor volume was about 70 mm³ with the normal saline as negative control. For LFP-D1 plus OPBP-1(8–12) treatment, we subcutaneously injected 2×10^6 H22 cells into the right flank of six-week-old female BALB/c mice purchased from Charles River. 3 mg/kg LFP-D1, 2.5 mg/kg OPBP-1(8–12), 3 mg/kg LFP-D1 plus 2.5 mg/kg OPBP-1(8–12), and 5.8 mg/kg LFOP (at the same molar dosage to 3 mg/kg LFP-D1) were administered every day when the tumor volume was about 50 mm³. For LFOP combined with RT treatment, the tumors were locally irradiated with 20 Gy with the tumor volume reached about 100 mm³ and 5.8 mg/kg LFOP was administered on the same day. The tumor volumes and body weights were recorded every two days during treatment for 14 days. Tumor volumes were calculated with Eq. (2):

$$V = 1/2 \times a \text{ (length)} \times b \text{ (width)} \times c \text{ (height)} \quad (2)$$

We also extracted the spleens and tumor-draining lymph nodes to conduct intracellular cytokine staining assay. The immunocytes were stimulated with 20 ng/mL PMA (P8139, Sigma, USA), 1 µmol/L ionomycin (407952, Sigma, USA) and seeded in 24 well plates at the density of 2×10^6 cells/well in the presence of Giogiplug protein transport inhibitor for 4 h at 37 °C. The secretion of IFN- γ from CD8⁺ and CD4⁺ T cells were analyzed

by flow cytometry. All animal experiments were under the approval of the Ethics Committee of Zhengzhou University with approval number ZZUIRB2021-32.

2.13. In vivo toxicity analysis

For H&E staining, mouse organs, including the heart, liver, spleen, lung and kidney, were fixed with 4% paraformaldehyde for 24 h. Tissues were then dehydrated and embedded in molten paraffin. The embedded tissues were sectioned, dewaxed, and stained with hematoxylin and eosin (H&E), and then visualized with microscope (Olympus).

For ALT/AST analysis, the mouse plasma samples were centrifuged to obtain supernatant ($1500 \times g$, 5 min, 4 °C) and we assessed the liver function by aminotransferase (AST) and alanine aminotransferase (ALT) kit (Nanjing Jiancheng Biological Engineering Research Institute, C010-2-1, C009-2-1, China).

2.14. Statistical analysis

Data were represented as means \pm standard error of mean (SEM) unless otherwise indicated, and statistical differences between two groups were evaluated with unpaired or paired Student's *t*-test. *P* values < 0.05 is considered to be significant difference. **P* < 0.05 , ***P* < 0.01 , and ****P* < 0.001 .

3. Results

3.1. LAG-3 and FGL1 are overexpressed in tumor tissues

By analyzing TCGA databases, we found that *LAG-3* is overexpressed in various tumor tissues (Fig. 1A), and higher than that of *PD-1* (Fig. 1B), especially in patients with renal cell carcinoma who respond to PD-1 mAb (Nivolumab) or not (Fig. 1C). The high expression of *LAG-3* was associated with poor prognosis in kidney clear cell carcinoma (KIRC), acute myeloid leukemia (LAML), uveal melanomas (UVM) and lung squamous cell carcinoma (LGG) using GEPIA (Supporting Information Fig. S1A). The single-cell sequencing data suggested that *LAG-3* mainly expressed in CD4⁺ and CD8⁺ T cells (Fig. 1D and E), consistent with the previous reports that *LAG-3* is an acknowledged exhaustion marker of effector T cells to maintain the immune suppression⁴⁶. Additionally, the *FGL1* expression is largely limited to the liver and pancreas (Fig. S1B) in human normal tissues according to The Human Protein Atlas, but the expression of *FGL1* is significantly upregulated in diverse human solid tumors including lung adenocarcinoma (LUAD), head and neck squamous cell carcinoma (HNSC) and prostate adenocarcinoma (PRAD) with analyzing TCGA databases (Fig. 1F). The further analysis focused on colorectal cancer observed that *FGL1* expressed higher in colorectal cancer tissues in GSE37182 dataset (Fig. 1G), GSE41328 dataset, GSE184093 dataset and GSE227550 dataset (Fig. S1D–S1F). More importantly, by analyzing the GSE128449 dataset, we observed that the expression level of *FGL1* was gradually upregulated during the tumor development from normal colon to polyps and primary tumors (Fig. 1H). The secretory *FGL1* comes from tumor cells rather than immunocyte according to The Human Protein Atlas (Fig. S1C). The high expression of *FGL1* was associated with poor prognosis in uterine carcinosarcoma (UCS), stomach adenocarcinoma

(STAD), lung squamous cell carcinoma (LUSC) and brain lower grade glioma (LGG) (Fig. S1G). The overexpressed *LAG-3* and *FGL1* in tumor tissues could induce resistance to PD-1 blockade treatment. This suggested the potential of targeting *LAG-3/FGL1* for cancer immunotherapy.

3.2. Screening of peptides blocking LAG-3/FGL1 interaction via phage display strategy and modification by D-amino acid substitution

We conducted phage display bio-panning and DNA sequencing⁴⁷ to select eight peptides named from LFP-1 to LFP-8 (Fig. 2A). The preliminary blocking assay was performed to assess the blocking efficacy of candidate peptides on human *LAG-3/FGL1* (Fig. 2B), and LFP-6 was most prominent with the IC₅₀ values of 11.32 ± 7.0 $\mu\text{mol/L}$ (Fig. 2C). Further, LFP-6 also effectively blocked mouse *LAG-3/FGL1* interaction in a dose-dependent manner with IC₅₀ of 47.2 ± 2.2 $\mu\text{mol/L}$ (Fig. 2D). The *K_D* values of LFP-6 peptide to human and mouse *LAG-3* determined by MST assay were 16.11 ± 5.5 $\mu\text{mol/L}$ and 14.63 ± 3.3 $\mu\text{mol/L}$, respectively (Fig. 2E and F). Considering the weak hydrolysis stability of LFP-6 composed with L-amino acids, we substituted it with D-amino acids from both N-terminal and C-terminal to extend the half-life and resistance to hydrolysis (detailed information is listed in Supporting Information Table S4). As a result, LFP-D1, LFP-D2 and LFP-D3 could retain the equivalent blocking activity compared to parental LFP-6 peptide at 200 $\mu\text{mol/L}$ (Fig. 2G). Subsequently, the blocking curves of LFP-D1 displayed optimal blocking activity toward both human and mouse *LAG-3/FGL1* with IC₅₀ values of 3.27 ± 0.4 $\mu\text{mol/L}$ and 17.46 ± 2.2 $\mu\text{mol/L}$, respectively (Fig. 2H and I). The dissociation curves of LFP-D1 to hLAG-3 and mLAG-3 were also tested by MST, and *K_D* values were 15.72 ± 6.7 $\mu\text{mol/L}$ and 10.91 ± 3.3 $\mu\text{mol/L}$, respectively (Fig. 2J and K). Besides, LFP-D1 did not affinity to both hFGL1 and mFGL1 (Supporting Information Fig. S2). Further, the enzymatic degradation stability was examined by incubating peptides with 10% human serum or MC38 tumor cell lines. Different from parental LFP-6 which was quickly degraded, LFP-D1 exhibited potent proteolysis resistance and retained the same initial concentration for up to 48 h (Fig. 2L and Supporting Information Fig. S3). Therefore, the peptide LFP-D1 with high blocking activity to *LAG-3/FGL1* was developed, which showed superior biological stability.

3.3. LFP-D1 promotes activation of T cells via blocking LAG-3/FGL1 interaction

Both *FGL1* and stable pMHC-II are important ligands of *LAG-3* to inhibit T cell proliferation and activation. It's clear that *LAG-3* can partially inhibit the activation of CD8⁺ and CD4⁺ T cells by interacting with stable pMHC-II expressed on APCs⁴⁸. Previously, our group generated a high affinity cyclic peptide C25 that showed a moderate blocking efficiency on *LAG-3/MHC-II* interaction³⁵. We tested the blocking and immunomodulatory ability of LFP-D1 and C25 peptides as showed in schematic diagram (Fig. 3A). LFP-D1 peptide almost completely abrogated the *LAG-3/FGL1* interaction rather than *LAG-3/MHC-II*, while C25 peptide efficiently inhibited the binding of *LAG-3/MHC-II* but not *LAG-3/FGL1* (Fig. 3B and C). Because *LAG-3* is highly homologous to CD4 in both amino

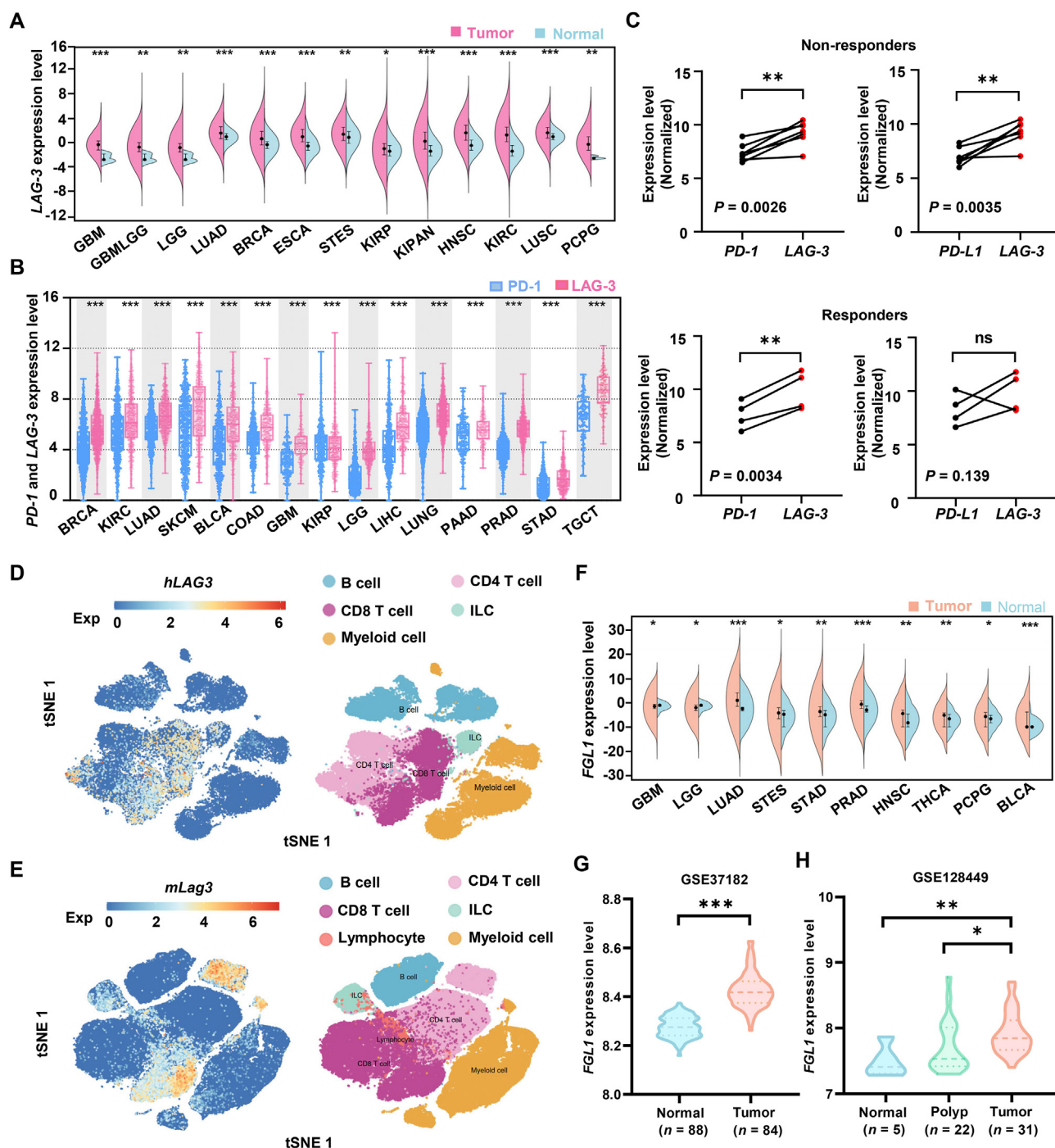


Figure 1 *LAG-3* and *FGL1* are overexpressed in tumor tissues. (A) Human *LAG-3* expression levels in different tumor types from TCGA database determined by Sangerbox (<http://sangerbox.com/home.html>). (B) Normalized *LAG-3* and *PD-1* expression across the tumors were analyzed with the data obtained from TCGA databases. (C) The expression of *PD-1*, *PD-L1* and *LAG-3* in human renal cell carcinoma samples of patients who response or not response to nivolumab in GSE67501 ($n = 7$). (D, E) t-SNE plot shows immune cell clusters (right) and the expression of *LAG3* (left) from human CRC (D) and MC38 mouse model (E) and all data comes from Single Cell RNA-seq Data Visualization and Analysis (<http://crlcukocyte.cancer-pku.cn/>). (F) The *FGL1* expression levels between normal tissue and tumor tissue analyzed by Sangerbox using TCGA databases. (G) The *FGL1* expression in normal tissues and colorectal cancer tissues in GSE37182 dataset. (H) The *FGL1* expression in normal tissues, polyps and colorectal cancer tissues in GSE128449 dataset. Statistical significance was determined by unpaired Student's *t*-test. * $P < 0.05$, ** $P < 0.01$, *** $P < 0.001$; ns, not significant.

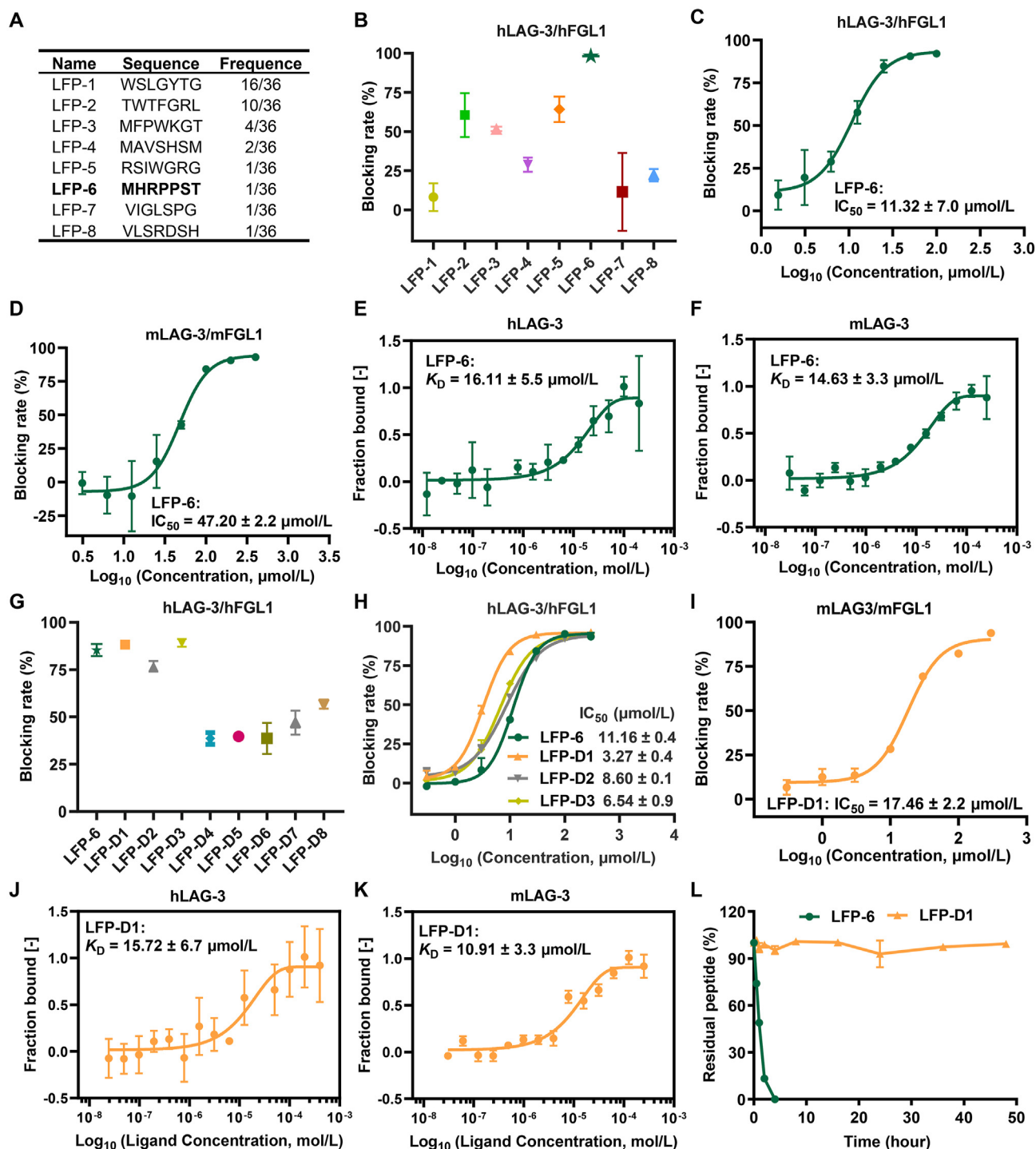


Figure 2 Screening of peptides blocking LAG-3/FGL1 interaction *via* phage display strategy and modification by D-amino acid substitution. (A) The sequences of candidate peptides targeting LAG-3 screened by phage peptide library. (B) The blocking efficacy of candidate peptides on interfering hLAG-3/hFGL1 at the concentration of 200 µmol/L. (C, D) The dose dependent blocking curves of LFP-6 on interfering hLAG-3/hFGL1 (C) and mLAG-3/mFGL1 interaction (D). (E, F) The dissociation curves and K_D values of LFP-6 to hLAG-3 (E) or mLAG-3 (F) measured by MST. (G) The residue of LFP-6 was substituted by D-amino acid with different methods, and the blocking activity was tested at the concentration of 200 µmol/L. (H) The dose-dependent blocking curves of LFP-6, LFP-D1, LFP-D2, LFP-D3 on interfering hLAG-3/hFGL1 interaction. (I) The ability of LFP-D1 to block mLAG-3/mFGL1 analyzed by flow cytometry. (J, K) The dissociation curves and K_D values of LFP-D1 to hLAG-3 (J) or mLAG-3 (K) determined by MST. (L) Residual peptides of LFP-6, LFP-D1 in 10% human serum at different time point analyzed by RP-HPLC. The representative data of three independent experiments are presented as mean \pm SEM.

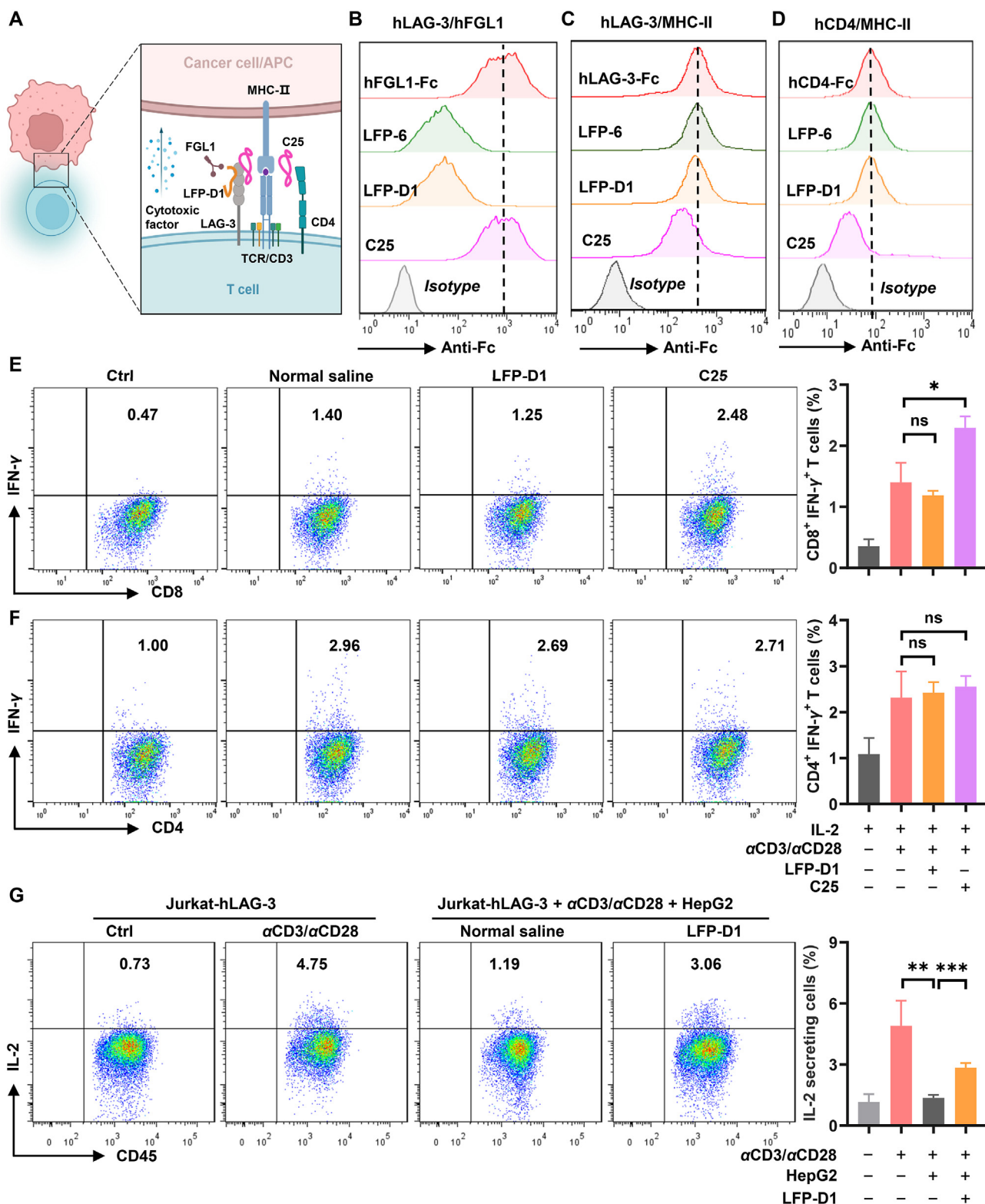


Figure 3 LFP-D1 promotes activation of T cells *via* blocking LAG-3/FGL1 interaction. (A) Schematic diagram of blocking and immunomodulatory ability of LFP-D1 and C25 peptides. (B)–(D) The blocking ability of LFP-6, LFP-D1 and C25 on LAG-3/FGL1 (B), LAG-3/MHC-II (C), and CD4/MHC-II (D) determined by flow cytometry. (E, F) The activated PBMC isolated from healthy donors were treated with NS, LFP-D1 or C25 for 72 h and the secretion of IFN- γ from CD8⁺ (E) and CD4⁺ T cells (F) was determined by flow cytometry ($n = 3$). (G) Jurkat-hLAG-3 stimulated with anti-CD3 and anti-CD28 stimulatory antibody cocultured with HepG2 cells in the presence of LFP-D1 or not ($n = 3$). The data are presented as mean \pm SEM and statistical significance was determined by unpaired Student's *t*-test. * $P < 0.05$, ** $P < 0.01$, *** $P < 0.001$; ns, not significant.

acid sequence and the shared ligand MHC-II, we assessed whether C25 interfered the interaction of recombinant human CD4 protein and MHC-II (HLA-DR) expressing on THP-1 cells, as predicted that C25 also partly block the interaction of recombinant protein CD4 to MHC-II while LFP-D1 has no blocking efficiency on it (Fig. 3D). These results indicate that C25 blocked the interaction of both LAG-3 and CD4 to MHC-II. Considering that CD4 discerning and binding to MHC-II was indispensable for the MHC-II/TCR complex to transmit stimulation signal⁴⁹, it raises the possibility that C25 antagonistic activity is ineffective in CD4⁺ T cells. To test this possibility, we treated PBMCs with anti-CD3 and anti-CD28 stimulatory antibodies. The IFN- γ production in CD8⁺ T cells was significantly enhanced in C25 group (Fig. 3E), while IFN- γ released by CD4⁺ T cells was hardly changed (Fig. 3F). Because the expression of FGL1 is largely limited to the liver, pancreas and tumor cells but not peripheral blood mononuclear cells (Fig. S1B and S1C), and without adding the recombinant FGL1 protein to the system. LFP-D1 peptide failed to augment the activation of both CD4⁺ and CD8⁺ T cells (Fig. 3E and F). This also evidenced LFP-D1 offered a better specificity and drug safety compared to C25 cycle peptide. Next, we investigated the immunomodulatory effect of LFP-D1 on Jurkat-hLAG-3 cells (Supporting Information Fig. S4A) when it cocultured with HepG2 cells that sufficiently expressed FGL1 (Fig. S4B and S4C). IL-2 production from Jurkat-hLAG-3 cells was partially suppressed when cocultured with HepG2 cells. Addition of LFP-D1 to the co-culture system effectively reversed the LAG-3-mediated reduction in IL-2 secretion (Fig. 3G). There is no significant difference in the secretion of IL-2 when Jurkat-hLAG-3 cells cocultured with SW620 cells that hardly express FGL1 (Fig. S4E) after treated with LFP-D1 for 48 h. All these results further supported that LFP-D1 specifically interfered the interaction of LAG-3/FGL1 and reversed the T cell suppression.

3.4. LFP-D1 restores antitumor T cell immune response and inhibits tumor growth

We next investigated the antitumor effects of LFP-D1. Primarily, MTT assay results showed LFP-D1 has no significant inhibitory effects on the proliferation and colony formation of MC38 mouse colon carcinoma cells (Supporting Information Fig. S5A, S5C and S5D). Next, MC38 cells were inoculated into C57BL/6 mice and the schematic of drug administration is showed in Fig. 4A. Upon the average tumor volume reached to 70 mm³, 1 mg/kg or 3 mg/kg LFP-D1 was intraperitoneal injected, with normal saline as negative control. The results showed LFP-D1 retarded the growth of MC38 tumors and high dose group showed more eminent antitumor activity (Fig. 4B and C). To analyze the correlation between the antitumor activity and the immunomodulatory effects of LFP-D1 peptide, we found that the ratio of tumor-infiltrating CD8⁺ T cells increased in LFP-D1 treated groups (Fig. 4D) and the percentages of IFN- γ producing CD8⁺ and CD4⁺ T cells in both tumor-draining lymph node (Fig. 4E) and spleen (Fig. 4F) were higher in LFP-D1 (3 mg/kg) group. As for toxicology, changes in body weight of tumor-bearing mice were similar among groups (Supporting Information Fig. S6A), as well the liver index (Fig. S6B), ALT (Fig. S6C) and AST level (Fig. S6D) in mice serum had no significant difference between LFP-D1 treatment and normal saline group. Collectively, these results indicate that the LAG-3/FGL1 blocking peptide LFP-D1 noticeably restored T cell activity and elicited antitumor response.

3.5. Design of dual blocking peptide LFOP interfering both LAG-3/FGL1 and PD-1/PD-L1 interaction

As the combination therapy of LAG-3 and PD-1 antibodies has shown significantly therapeutic effects, which is superior than blocking alone in clinic, we designed a bispecific peptide LFOP peptide by conjugating LFP-D1 and PD-1/PD-L1 blocking peptide OPBP-1(8–12) with a flexible linker (GS)³⁷. The molecular weight and purity of peptide was determined by mass spectrum and RP-HPLC (Supporting Information Fig. S7). Next, the binding affinity, blocking efficacy and immune activity of LFOP were tested (Fig. 5A). The primary blocking efficacy of LFOP to both human LAG-3/FGL1 and PD-1/PD-L1 were in line with its parental peptide (Fig. 5B and C). Further, the blocking activity of LFOP to human LAG-3/FGL1 with IC₅₀ value of 1.57 \pm 0.2 μ mol/L (Fig. 5D) was superior than its parental peptide LFP-D1 with IC₅₀ value of 3.27 \pm 0.4 μ mol/L (Fig. 2H), while the binding affinity to LAG-3 was conserved (Fig. 5E). For PD-1/PD-L1 pathway, LFOP maintained the blocking efficacy and the binding affinity to PD-L1 compared to its parental peptide OPBP-1(8–12) (Fig. 5F and G). The similar binding and blocking assays were also performed in mouse system (Supporting Information Fig. S8).

To further assess the T cell activation potential of LFOP in physiological conditions, we treated primary human PBMCs or mouse splenocytes with anti-CD3 and anti-CD28 stimulatory antibodies and cocultured with tumor cells. Firstly, we investigated the ability of LFOP to promote human T cell response *in vitro* by mixing stimulated PBMCs expressing LAG-3 and PD-1 with HepG2 cells endogenously expressing FGL1 and PD-L1 (Fig. S4B–S4D), which induced a robust suppression on T cell in LAG-3 and PD-1 dependent manner. As expected, blockade of either LAG-3 or PD-L1 can induce IFN- γ secretion and augment proliferation of human CD8⁺ and CD4⁺ T cells, but the dual blockade antagonist LFOP exhibited the greater T cell immune response reached the same therapeutic effect as the combination group (Fig. 5H–K), indicating a synergistic effect compared with blockade alone. Subsequently, we analyzed the effect of LFOP on mouse splenocytes and cocultured them with MC38 cells for 72 h in the presence of recombinant IL-2, anti-CD3 and anti-CD28 stimulatory antibodies. We observed LFOP induced the significant increase of IFN- γ and proliferative CD8⁺ and CD4⁺ T cells compared with blockade either LAG-3 or PD-L1 alone (Supporting Information Fig. S9). We also did additional H22 mouse liver cancer model to further detect the effect of LFOP. Results suggest that LFOP treatment significantly inhibited the tumor growth (Supporting Information Fig. S10). All indicated that the bispecific peptide LFOP interfering LAG-3 and PD-L1 pathways as well promoted the activation of effector T cells.

3.6. Upregulation of immune checkpoints in tumor microenvironment following radiotherapy

Recent studies indicated localized irradiation (IR) mediate local and distant tumor regression in a T cell dependent manner, but the engagement of T cell negative regulatory pathway such as PD-1 and LAG-3 axis often inhibit the function of T cell³⁹. Here, we firstly observed that the expression of *Fgl1* (Fig. 6A) and *Pd-l1* (Fig. 6B and C) were upregulated over time in MC38 cells after 10 Gy IR. Then, we resected the MC38 tumor tissues 3 days after radiation with 20 Gy and analyzed the expression of LAG-3, PD-1

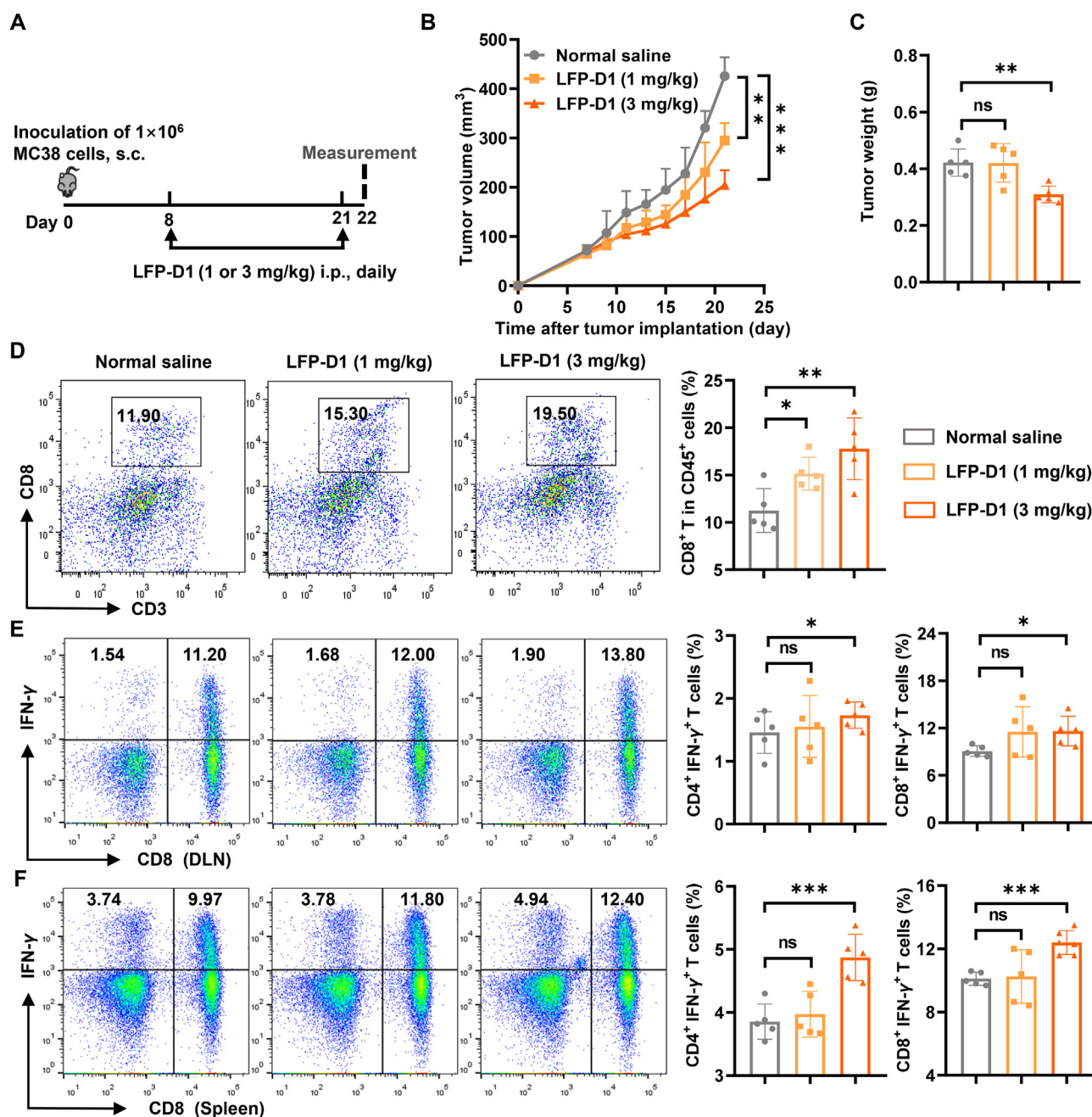


Figure 4 LFP-D1 restores antitumor T-cell immune response and inhibits tumor growth. (A) Schematic of LFP-D1 treatment on MC38 tumor model. LFP-D1 was injected intraperitoneally in mice daily for 14 days. (B) Tumor growth curve of MC38 tumor-bearing mice treated with saline or LFP-D1 peptide ($n = 5$). (C) Statistical analysis of tumor weight between different groups after treated for 14 days ($n = 5$). (D) The frequencies of intratumoral CD8⁺ T cells in CD45⁺ lymphocytes were analyzed ($n = 5$). (E, F) Cells from the tumor-draining lymph nodes (E) or spleens (F) were obtained and stimulated with 20 ng/mL of PMA and 1 $\mu\text{mol/L}$ ionomycin containing protein transport inhibitor for 4 h. IFN- γ -secreting CD8⁺ T (CD45⁺CD3⁺CD8⁺) and CD4⁺ T cells (CD45⁺CD3⁺CD8⁻) were detected by flow cytometry ($n = 5$). Data are represented as mean \pm SEM and statistical significance was determined by unpaired Student's *t*-test. * $P < 0.05$, ** $P < 0.01$, *** $P < 0.001$; ns, not significant.

and PD-L1 in the tumor microenvironment by flow cytometry. As shown in Fig. 6D, the PD-L1 expression on tumor cells (CD45⁺) was remarkably increased in comparison to non-irradiated control tumors. Next, the expression of PD-1 and LAG-3 were determined on CD8⁺ and CD4⁺ T cells from peripheral blood and tumor-infiltrated immunocytes. PD-1 expression in peripheral blood CD8⁺ and CD4⁺ T cells did not change while it was elevated on

tumor-infiltrated T cells (Fig. 6E). As to LAG-3, increased expression in CD8⁺ and CD4⁺ T cells after IR was evidenced although untreated tumors had unapparent baseline LAG-3 expression levels (Fig. 6F). These data indicate that alteration of the LAG-3/FGL1 and PD-L1/PD-1 axis in the tumor microenvironment might inhibit T cell function and reduce the therapeutic effect of radiotherapy.

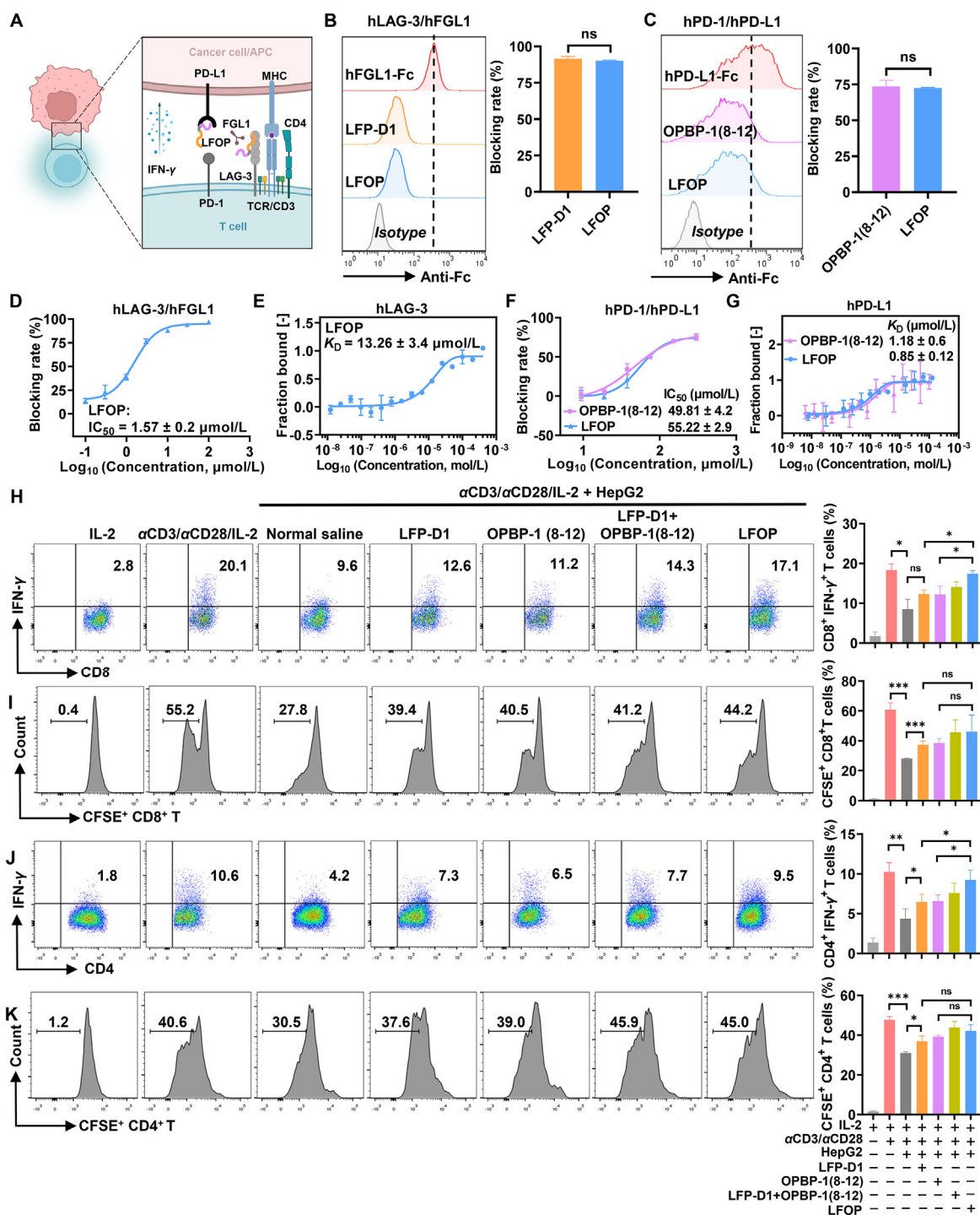


Figure 5 Design of dual blocking peptide LFOF interfering both LAG-3/FGL1 and PD-1/PD-L1 interaction. (A) Structure diagram of LFOF blocking both LAG-3/FGL1 and PD-1/PD-L1 interaction to restore the function of T cells. (B) Blocking efficacy of LFP-D1 and LFOF on hLAG-3/hFGL1 interaction at the concentration of 100 $\mu\text{mol/L}$ ($n = 3$). (C) Blocking efficacy of OPBP-1(8-12) and LFOF on hPD-1/hPD-L1 interaction at the concentration of 100 $\mu\text{mol/L}$ ($n = 3$). (D) The dose-dependent blocking curves of LFOF interfering hLAG-3/hFGL1 interaction ($n = 3$). Data are represented as mean \pm SD. (E) The binding affinity of LFOF to hLAG-3 determined by MST ($n = 3$). (F) The dose-dependent blocking curves of OPBP-1(8-12) and LFOF interfering hPD-1/hPD-L1 interaction ($n = 3$). (G) The affinity of OPBP-1(8-12) and LFOF to hPD-L1 determined by MST ($n = 3$). (H)–(K) The PBMCs isolated from healthy donors stained with CFSE and cocultured with HpeG2 cells for 72 h in the presence of LFP-D1, OPBP-1(8-12), LFP-D1 plus OPBP-1(8-12) or LFOF at the concentration of 100 $\mu\text{mol/L}$. IFN- γ -secreting CD8 $^+$ T cells (H), and the proliferation of CD8 $^+$ T cells (I), and IFN- γ -secreting CD4 $^+$ T cells (J), and the proliferation of CD4 $^+$ T cells (K) were detected by flow cytometry ($n = 3$). Data are represented as mean \pm SEM. Statistical significance was determined by unpaired Student's t -test. * $P < 0.05$, ** $P < 0.01$, *** $P < 0.001$; ns, not significant.

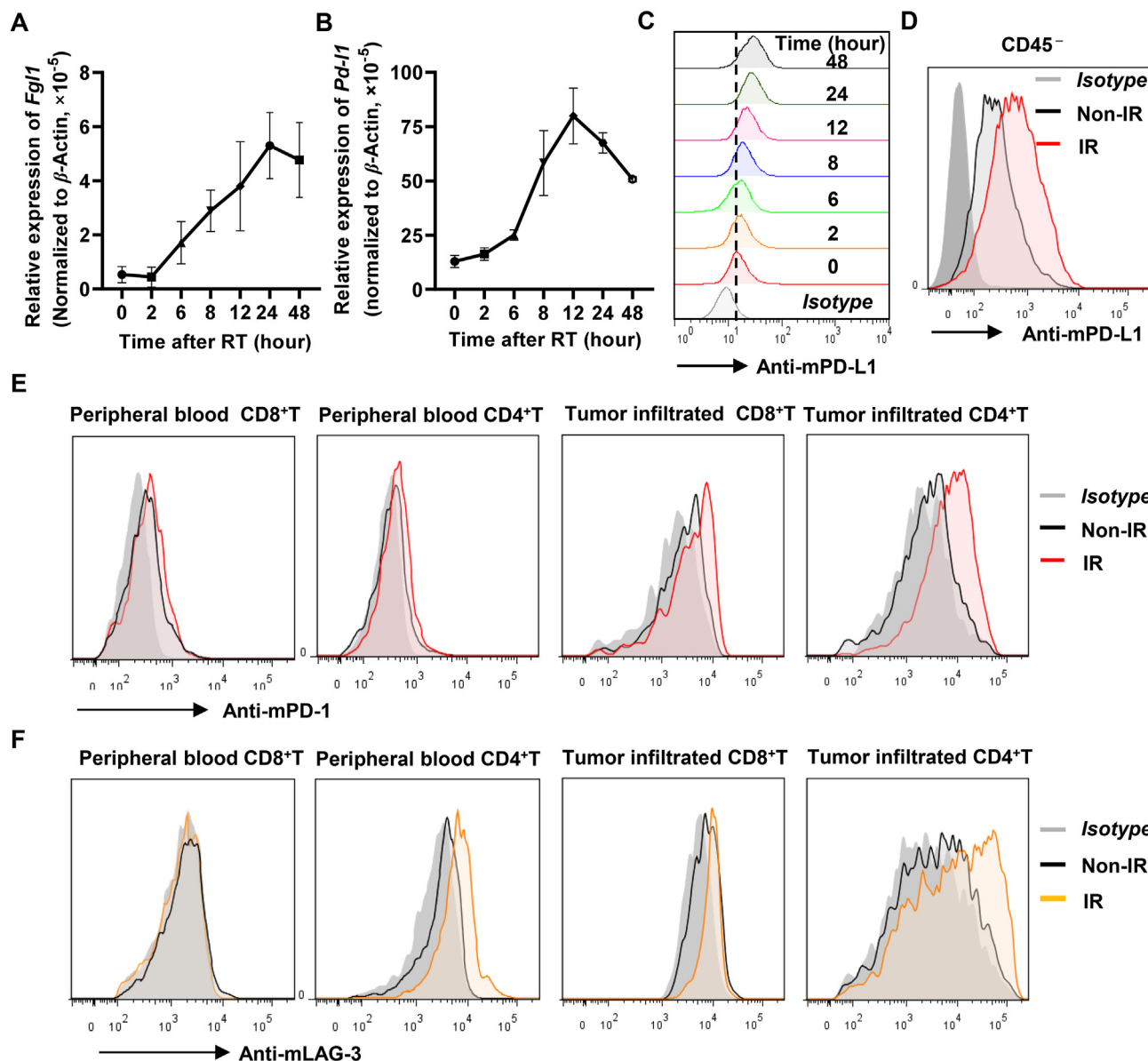


Figure 6 Upregulation of immune checkpoints in tumor microenvironment following radiotherapy. (A–C) The expression levels of *Fgl1* (A) and *Pd-I1* (B) in MC38 cells detected by qPCR or flow cytometry (C) after radiotherapy with 10 Gy ($n = 3$). (D) The expression of PD-L1 increased in MC38 tumor cells (CD45⁻ cells) after radiotherapy with 20 Gy. (E, F) Flow cytometry was used to detect the expression of PD-1 (E) or LAG-3 (F) on CD4⁺ and CD8⁺ T cells in peripheral blood or tumor infiltrated T cells from MC38 tumor-bearing mice after radiotherapy with 20 Gy. The data are presented as mean \pm SEM.

3.7. Combination of LFOP with radiotherapy synergistically inhibits tumor growth

IR-induced upregulation of LAG-3/FGL1 and PD-1/PD-L1 axes provide an opportunity for co-blockade of LAG-3/PD-L1 combined with RT treatment that will uncover the stronger cytotoxic potential of host immunity against tumor. We tested the potential of LFOP synergy with RT to alleviate the inhibitory action of T cells and facilitate tumor regression. Firstly, MTT assay showed LFOP has no impact on the proliferation and colony formation of MC38 cells (Fig. S5B and S5C). The MC38 tumor-bearing mice were treated with a local 20 Gy IR when the tumors reached approximately 100 mm³, and then treated with or without LFOP

(Fig. 7A). Surprisingly, LFOP or RT alone slowed tumor progression, whereas the combination treatment effectively controlled tumor growth even partial regression (Fig. 7B and C). Next, to determine whether LFOP and RT treatment engaged antitumor immune response, the cells from the tumor tissues, tumor-draining lymph nodes and spleens were obtained after treatment. The proportion of intertumoral CD8⁺ T cells (Fig. 7D) and CD4⁺ T cells (Fig. 7E) in LFOP and RT groups significantly increased compared with the control group, but the LFOP and RT combination group could most remarkably increase the infiltration of T cells. Moreover, the proportions of IFN- γ ⁺ CD8⁺ T cells and IFN- γ ⁺ CD4⁺ T cells in spleens and tumor-draining lymph nodes were increased both in LFOP and IR group, but highest increment was

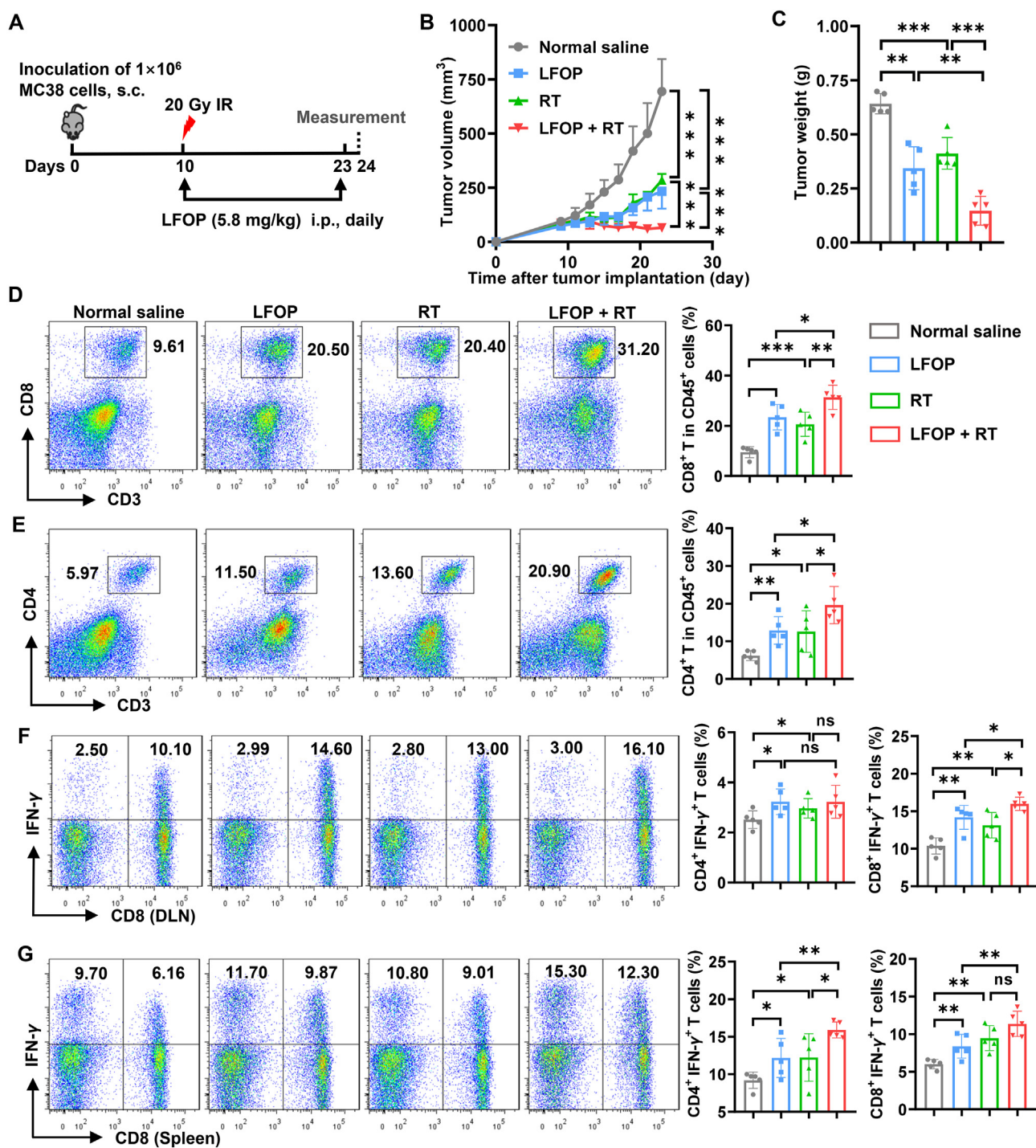


Figure 7 Combination of LFOP with radiotherapy synergistically inhibits tumor growth. (A) Schematic diagram of LFOP and radiotherapy combination therapy in MC38 tumor model. (B) Tumor growth curve of MC38 tumor-bearing mice treated with normal saline, RT, LFOP or LFOP combined with RT ($n = 5$). (C) Statistical analysis of tumor weight between different groups after treated for 14 days ($n = 5$). (D, E) The frequencies of intratumoral CD8⁺ T cells (D) and CD4⁺ T cells (E) in CD45⁺ lymphocytes were analyzed ($n = 5$). (F, G) Lymphocytes from the tumor-draining lymph nodes (F) and spleen (G) were obtained and stimulated with 20 ng/mL of PMA and 1 $\mu\text{mol/L}$ ionomycin containing protein transport inhibitor for 4 h. IFN- γ -secreting CD8⁺ T (CD45⁺CD3⁺CD8⁺) and CD4⁺ T cells (CD45⁺CD3⁺CD8⁻) were detected by flow cytometry ($n = 5$). Data are represented as mean \pm SEM and statistical significance was determined by unpaired Student's *t*-test. * $P < 0.05$, ** $P < 0.01$, *** $P < 0.001$; ns, not significant.

observed in the combination group (Fig. 7F and G). Here, we also conducted the toxicity analysis. The body weight of the mice among groups showed no significant differences at ultimate time in spite of some slight body weight loss after IR (Supporting Information Fig. S11A). Besides, ALT and AST levels in serum were indistinguishable (Fig. S11B and S11C). Histopathology analysis illustrated no abnormalities by H&E staining tissue sections from major organs after treatment (Fig. S11D). Consistently, these results demonstrated that the combination of LAG-3 and PD-L1 bispecific peptide LFOP with IR could be a very promising strategy to synergistically eradicate the tumor through activating T cell response.

4. Discussion

Considering anti-PD-1/PD-L1 treatment low response rates and resistance, alternative immune checkpoints are desperately needed. LAG-3 is a promising immune checkpoint, which expresses in activated TILs with continuous antigenic stimulation, often in parallel with increased PD-1 and is involved in the process of T cell exhaustion. Targeting LAG-3 is the novel direction for clinical trials and combination with other treatment strategies significantly improve clinical efficacy. Wherein, Relatlimab and Nivolumab are approved by FDA in unresectable or metastatic melanoma with improved disease-free survival⁵⁰. Combination of LAG-3 inhibitors with PD-1/PD-L1 or other checkpoints inhibitors also have been extensively explored in various cancers in clinic^{51,52}.

Wang et al.¹⁷ identified and characterized FGL1 is the major ligand of LAG-3. The interaction sites between the FD region of FGL1 and the D1–D2 region of LAG-3 were non-redundant with MHC-II/LAG-3 binding sites. More importantly, FGL1 presented inhibitory functional role in a LAG-3 dependent manner by suppressing the production of cytokine from 3A9-hLAG-3 cells and activated T cells *in vitro*, as well specifically abrogating the interaction of LAG-3/FGL1 effectively retarding the tumor growth and immune evasion in colorectal cancer¹⁷, breast cancer²⁸ and liver cancer mouse model. However, a recent study contradicted with it and insisted that it was stable pMHC-II, but not FGL1, served as the sole functional ligand of LAG-3 to trigger its inhibitory function⁴⁸. Wherein, Takumi Maruhashi et al.⁴⁸ manifested that C9B7W antibody blocked both the bindings of stable pMHC-II and FGL1 to LAG-3, which was inconsistent with Wang's and Workman's studies¹⁷. Meanwhile, they insisted that addition of recombinant FGL1 protein failed to induce or augment the inhibitory effect of LAG-3 on T cell activation *in vitro*, which may result from the differences of the biochemical properties of the purified protein. However, they did not assess the immunosuppression of FGL1 in mouse tumor model by specific blocking LAG-3/FGL1 mAbs or LAG-3 gene mutant mice. Recently, the crystal structure and biochemical studies of LAG-3 and FGL1 showed that the low concentrations of FGL1 induced the cluster of LAG-3 on the cell membrane surface, which is the primary basis for LAG-3 inhibitory function¹⁴. Besides, Thudium et al.⁵³ suggested the engineered co-expression FGL1 and MHC-II in APC cells resulted in more potent inhibition of T cell responsiveness compared with engagement of MHC-II alone. It remains to be determined what the physical oligomerization state of FGL1 is in the periphery blood and the TME, and it remains unclear what mechanism FGL1 functionally engage with LAG-3 to inhibit T cells.

We assumed FGL1 was the major inhibitory ligand for LAG-3. In this study, for the first time, we developed the peptide

LFP-D1 specifically blocked LAG-3/FGL1 interaction, but not LAG-3/MHC-II interaction, and which promoted the proliferation and functional activation of both CD4⁺ and CD8⁺ T cells when cocultured them with tumor cells *in vitro*. Meanwhile, LFP-D1 effectively delayed the tumor growth of MC38 tumors *in vivo*, and promoted the infiltration of CD8⁺ T cells into tumors, and elicited the potent systematic immune response by increasing production of IFN- γ from CD4⁺ and CD8⁺ T cells in both tumor-draining lymph nodes and spleens. We also observed the ratio of intratumoral M1/M2 macrophage increased in LFP-D1 groups in comparison to normal saline group (data not shown). With neither LAG-3 nor FGL1 is expressed on macrophages, we considered that LFP-D1 altered the phenotype and function of immunocytes in tumor microenvironment. One possible mechanism might be the increase of IFN- γ , which is the putative cytokine to induce M1 phenotype of macrophages.

In the previous study, our group developed C25 peptide, selectively blocking the interaction of LAG-3/MHC-II, but not LAG-3/FGL1³⁵. But C25 also blocked the binding of CD4/MHC-II, which inhibited the effective activation of CD4⁺ T cells, while LFP-D1 can simultaneously activated the functions of CD8⁺ and CD4⁺ T cells both *in vivo* and *in vitro*, which is consistent with Wang's research¹⁷. The signal and functional differences between FGL1 and MHC-II binding to LAG-3 remain obscured. Whether combination with C25 blockade can enhance the antitumor effect of LFP-D1 remains to be further explored. Generally, these data support that both FGL1 and MHC-II are the inhibitory ligand of LAG-3.

In recent years, preclinical data illustrate a clear synergy between the inhibitory receptors LAG-3 and PD-1 in controlling immune evasion and immune tolerance^{54,55}. Combined strategies with blocking antibodies against LAG-3 and PD-1 receptors result in more robust immune responses than either single agent treatment²⁵. Moreover, LAG-3/FGL1 interaction is non-redundant for PD-1/PD-L1 pathway, and higher plasma FGL1 levels are associated with worse overall survival in NSCLC and metastatic melanoma patients treated with anti-PD-1¹⁷. There is an intense competition among pharmaceutical companies to develop LAG-3 antibodies and evaluate the antitumor effects in various cancer types as monotherapy or combined with PD-1/PD-L1 antibodies. To date, relatlimab is the first LAG-3 antibody approved by FDA to combine with nivolumab for unresectable or metastatic melanoma patients⁵¹, which block the interaction of LAG-3 with both MHC-II and FGL1⁵³. Herein, we designed the bispecific peptide LFOP binding to LAG-3 and PD-L1 proteins with the similar affinity to its parental peptides. Similarly, in the primary T cell cocultured with tumor cells assay, we tested the proliferation and secretion of IFN- γ from T cells, while only modest activity was observed under single blockade LAG-3/FGL1 with LFP-D1 or PD-1/PD-L1 with OPBP-1(8–12), compared with the substantially enhanced responsiveness in the context of co-blockade of LAG-3 and PD-L1 with LFOP. Differences in the intracellular inhibitory signaling and expression profiles of these two molecules partly explain the synergistic effect but the exact mechanisms still need further exploration.

Numerous reviews indicate that radiotherapy could increase the treatment efficacy of immune checkpoint therapy and reprogram tumor microenvironment by releasing tumor-associated antigens and chemokines, recruiting the activated cytotoxic lymphocytes to infiltrate into the tumor⁵⁶. Meanwhile, radiotherapy also increases the expression of negative immune

checkpoints, which also enhances immunosuppression⁵⁷. Our study showed that radiotherapy upregulated the expression of LAG-3 and PD-1 in TILs and PD-L1 in tumor cells (CD45⁺) in MC38 tumors after RT. Also, the upregulation of FGL1 was observed in MC38 cells after radiotherapy, which has showed positive correlation with radiation dose in liver⁴². LFOP combined with radiotherapy has significant antitumor activity in MC38 tumors-bearing mice, not only remarkably suppressed tumor growth but part of tumors regressed along with increased tumor-infiltrating CD8⁺ and CD4⁺ T cells. As we know, LAG-3 highly expresses in Tregs cells and transmits signals to conduct their function and proliferation⁵⁸, and radiotherapy was associated with increased Tregs in tumor microenvironment⁵⁹. We also detected the decreased Tregs after treatment with LFOP (data not shown). Radiotherapy combined with immune checkpoint therapy can also increase the proportion of memory cells in immune organs, resulting in remote effects and systemic immunity. The effect of combination of LFOP with radiotherapy on memory cells has not been verified. This study indicates that LFOP could address radiation-induced immunosuppression and also further boost the activation of antitumor immunity by dual blockade of PD-1/PD-L1 and LAG-3/FGL1 pathway.

5. Conclusions

Collectively, LAG-3 and FGL1 are overexpressed in various cancers and negatively regulate immune response. We screened and developed LFP-D1 peptide targeting LAG-3 by high-throughput phage display technology and substituted with D-amino acid, which specifically interfered the interaction of LAG-3 and FGL1 and enhanced the antitumor efficacy. The bispecific peptide LFOP inhibited both PD-1/PD-L1 and LAG-3/FGL1 pathways and further increased the infiltration and function of T lymphocytes when combined with radiotherapy.

Acknowledgments

This work was supported by the grants from National Science Foundation of China (U20A20369). “Pearl River Talent Plan” Innovation and Entrepreneurship Team Project of Guangdong Province (2019ZT08Y464, China), Guangdong Basic and Applied Basic Research Foundation (2022B1515120085, China), Shenzhen Science and Technology Program (KQTD20190929173853397, China) and Henan Provincial Key R&D and Promotion Special (Scientific Problem Tackling) (222102310344, China).

Author contributions

Yanfeng Gao and Wenjie Zhai conceived and designed the experiments. Yuzhen Qian and Yixuan Sun performed the experiments, Peishang Shi, Xiuman Zhou, Qiongqiong Zhang, Qingyu Dong, Shengzhe Jin, Lu Qiu, Xiaoshuang Niu, Xiaowen Zhou helped to perform the experiments. Yuzhen Qian, Yixuan Sun, Wenshan Zhao, Yahong Wu, Wenjie Zhai, Yanfeng Gao analyzed and interpreted the results. All authors revised the manuscript, discussed the results and gave final approval of the manuscript.

Conflicts of interest

The authors declare no conflicts of interest.

Appendix A. Supporting information

Supporting data to this article can be found online at <https://doi.org/10.1016/j.apsb.2023.12.011>.

References

- Hargadon KM, Johnson CE, Williams CJ. Immune checkpoint blockade therapy for cancer: an overview of FDA-approved immune checkpoint inhibitors. *Int Immunopharm* 2018;**62**:29–39.
- Kordbacheh T, Honeychurch J, Blackhall F, Faivre-Finn C, Illidge T. Radiotherapy and anti-PD-1/PD-L1 combinations in lung cancer: building better translational research platforms. *Ann Oncol* 2018;**29**:301–10.
- Yi M, Zheng X, Niu M, Zhu S, Ge H, Wu K. Combination strategies with PD-1/PD-L1 blockade: current advances and future directions. *Mol Cancer* 2022;**21**:28.
- Havel JJ, Chowell D, Chan TA. The evolving landscape of biomarkers for checkpoint inhibitor immunotherapy. *Nat Rev Cancer* 2019;**19**:133–50.
- Kubli SP, Berger T, Araujo DV, Siu LL, Mak TW. Beyond immune checkpoint blockade: emerging immunological strategies. *Nat Rev Drug Discov* 2021;**20**:899–919.
- Budimir N, Thomas GD, Dolina JS, Salek-Ardakani S. Reversing T-cell exhaustion in cancer: lessons learned from PD-1/PD-L1 immune checkpoint blockade. *Cancer Immunol Res* 2022;**10**:146–53.
- Andrews LP, Marciscano AE, Drake CG, Vignali DA. LAG3 (CD223) as a cancer immunotherapy target. *Immunol Rev* 2017;**276**:80–96.
- Das M, Zhu C, Kuchroo VK. Tim-3 and its role in regulating anti-tumor immunity. *Immunol Rev* 2017;**276**:97–111.
- Qin S, Xu L, Yi M, Yu S, Wu K, Luo S. Novel immune checkpoint targets: moving beyond PD-1 and CTLA-4. *Mol Cancer* 2019;**18**:155.
- Ge Z, Peppelenbosch MP, Sprengers D, Kwekkeboom J. TIGIT, the next step towards successful combination immune checkpoint therapy in cancer. *Front Immunol* 2021;**12**:699895.
- Workman CJ, Cauley LS, Kim JJ, Blackman MA, Woodland DL, Vignali DA. Lymphocyte activation gene-3 (CD223) regulates the size of the expanding T cell population following antigen activation *in vivo*. *J Immunol* 2004;**172**:5450–5.
- Workman CJ, Wang Y, El Kasmī KC, Pardoll DM, Murray PJ, Drake CG, et al. LAG-3 regulates plasmacytoid dendritic cell homeostasis. *J Immunol* 2009;**182**:1885–91.
- Triebel F, Jitsukawa S, Baixeras E, Roman-Roman S, Genevée C, Viegas-Pequignot E, et al. LAG-3, a novel lymphocyte activation gene closely related to CD4. *J Exp Med* 1990;**171**:1393–405.
- Ming Q, Celiás DP, Wu C, Cole AR, Singh S, Mason C, et al. LAG3 ectodomain structure reveals functional interfaces for ligand and antibody recognition. *Nat Immunol* 2022;**23**:1031–41.
- MacLachlan BJ, Mason GH, Greenshields-Watson A, Triebel F, Gallimore A, Cole DK, et al. Molecular characterization of HLA class II binding to the LAG-3 T cell co-inhibitory receptor. *Eur J Immunol* 2021;**51**:331–41.
- Workman CJ, Vignali DA. The CD4-related molecule, LAG-3 (CD223), regulates the expansion of activated T cells. *Eur J Immunol* 2003;**33**:970–9.
- Wang J, Sanmamed MF, Datar I, Su TT, Ji L, Sun J, et al. Fibrinogen-like protein 1 is a major immune inhibitory ligand of LAG-3. *Cell* 2019;**176**:334–47.
- Wu HT, Ou HY, Hung HC, Su YC, Lu FH, Wu JS, et al. A novel hepatokine, HFREPI, plays a crucial role in the development of insulin resistance and type 2 diabetes. *Diabetologia* 2016;**59**:1732–42.
- Li CY, Cao CZ, Xu WX, Cao MM, Yang F, Dong L, et al. Recombinant human hepassocin stimulates proliferation of hepatocytes *in vivo* and improves survival in rats with fulminant hepatic failure. *Gut* 2010;**59**:817–26.
- Ou HY, Wu HT, Lin CH, Du YF, Hu CY, Hung HC, et al. The hepatic protection effects of hepassocin in hyperglycemic crisis. *J Clin Endocrinol Metab* 2017;**102**:2407–15.

21. Wu HT, Chen SC, Fan KC, Kuo CH, Lin SY, Wang SH, et al. Targeting fibrinogen-like protein 1 is a novel therapeutic strategy to combat obesity. *Faseb J* 2020;**34**:2958–67.
22. Sun XL, Qiao LC, Gong J, Wen K, Xu ZZ, Yang BL. Proteomics identifies a novel role of fibrinogen-like protein 1 in Crohn's disease. *World J Gastroenterol* 2021;**27**:5946–57.
23. Guo M, Yuan F, Qi F, Sun J, Rao Q, Zhao Z, et al. Expression and clinical significance of LAG-3, FGL1, PD-L1 and CD8⁺T cells in hepatocellular carcinoma using multiplex quantitative analysis. *J Transl Med* 2020;**18**:306.
24. Qian W, Zhao M, Wang R, Li H. Fibrinogen-like protein 1 (FGL1): the next immune checkpoint target. *J Hematol Oncol* 2021;**14**:147.
25. Jiang H, Ni H, Zhang P, Guo X, Wu M, Shen H, et al. PD-L1/LAG-3 bispecific antibody enhances tumor-specific immunity. *Oncol Immunology* 2021;**10**:1943180.
26. Kim YJ, Won CH, Lee MW, Choi JH, Chang SE, Lee WJ. Correlation between tumor-associated macrophage and immune checkpoint molecule expression and its prognostic significance in cutaneous melanoma. *J Clin Med* 2020;**9**:2500.
27. Wan WJ, Huang G, Wang Y, Tang Y, Li H, Jia CH, et al. Coadministration of iRGD peptide with ROS-sensitive nanoparticles co-delivering siFGL1 and siPD-L1 enhanced tumor immunotherapy. *Acta Biomater* 2021;**136**:473–84.
28. Gong C, Yu X, Zhang W, Han L, Wang R, Wang Y, et al. Regulating the immunosuppressive tumor microenvironment to enhance breast cancer immunotherapy using pH-responsive hybrid membrane-coated nanoparticles. *J Nanobiotechnol* 2021;**19**:58.
29. Gong L, Zhao H, Liu Y, Wu H, Liu C, Chang S, et al. Research advances in peptide–drug conjugates. *Acta Pharm Sin B* 2023;**13**:3659–77.
30. Chang HN, Liu BY, Qi YK, Zhou Y, Chen YP, Pan KM, et al. Blocking of the PD-1/PD-L1 interaction by a D-peptide antagonist for cancer immunotherapy. *Angew Chem Int Ed Engl* 2015;**54**:11760–4.
31. Zhou X, Zuo C, Li W, Shi W, Zhou X, Wang H, et al. A novel D-peptide identified by mirror-image phage display blocks TIGIT/PVR for cancer immunotherapy. *Angew Chem Int Ed Engl* 2020;**59**:15114–8.
32. Wang H, Sun Y, Zhou X, Chen C, Jiao L, Li W, et al. CD47/SIRP α blocking peptide identification and synergistic effect with irradiation for cancer immunotherapy. *J Immunother Cancer* 2020;**8**:000905.
33. Li X, Gohain N, Chen S, Li Y, Zhao X, Li B, et al. Design of ultrahigh-affinity and dual-specificity peptide antagonists of MDM2 and MDMX for P53 activation and tumor suppression. *Acta Pharm Sin B* 2021;**11**:2655–69.
34. Hu C, Song Y, Zhang Y, He S, Liu X, Yang X, et al. Sequential delivery of PD-1/PD-L1 blockade peptide and Ido inhibitor for immunosuppressive microenvironment remodeling via an MMP-2 responsive dual-targeting liposome. *Acta Pharm Sin B* 2023;**13**:2176–87.
35. Zhai W, Zhou X, Wang H, Li W, Chen G, Sui X, et al. A novel cyclic peptide targeting LAG-3 for cancer immunotherapy by activating antigen-specific CD8⁺ T cell responses. *Acta Pharm Sin B* 2020;**10**:1047–60.
36. Li W, Zhu X, Zhou X, Wang X, Zhai W, Li B, et al. An orally available PD-1/PD-L1 blocking peptide OPBP-1-loaded trimethyl chitosan hydrogel for cancer immunotherapy. *J Control Release* 2021;**334**:376–88.
37. Jiao L, Dong Q, Zhai W, Zhao W, Shi P, Wu Y, et al. A PD-L1 and VEGFR2 dual targeted peptide and its combination with irradiation for cancer immunotherapy. *Pharmacol Res* 2022;**182**:106343.
38. Weichselbaum RR, Liang H, Deng L, Fu YX. Radiotherapy and immunotherapy: a beneficial liaison?. *Nat Rev Clin Oncol* 2017;**14**:365–79.
39. Jing W, Gershan JA, Weber J, Tlomak D, McOlash L, Sabatos-Peyton C, et al. Combined immune checkpoint protein blockade and low dose whole body irradiation as immunotherapy for myeloma. *J Immunother Cancer* 2015;**3**:2.
40. Deng L, Liang H, Burnette B, Beckett M, Darga T, Weichselbaum RR, et al. Irradiation and anti-PD-L1 treatment synergistically promote antitumor immunity in mice. *J Clin Invest* 2014;**124**:687–95.
41. Hwang WL, Pike LRG, Royce TJ, Mahal BA, Loeffler JS. Safety of combining radiotherapy with immune-checkpoint inhibition. *Nat Rev Clin Oncol* 2018;**15**:477–94.
42. Han NK, Jung MG, Jeong YJ, Son Y, Han SC, Park S, et al. Plasma fibrinogen-like 1 as a potential biomarker for radiation-induced liver injury. *Cells* 2019;**8**:1042.
43. Jin H, Kang GY, Jeon S, Kim JM, Park YN, Cho J, et al. Identification of molecular signatures involved in radiation-induced lung fibrosis. *J Mol Med (Berl)* 2019;**97**:37–47.
44. Chen G, Feng Y, Sun Z, Gao Y, Wu C, Zhang H, et al. mRNA and lncRNA expression profiling of radiation-induced gastric injury reveals potential radiation-responsive transcription factors. *Dose Response* 2019;**17**:1559325819886766.
45. Sun Y, Qian Y, Chen C, Wang H, Zhou X, Zhai W, et al. Extracellular vesicle IL-32 promotes the M2 macrophage polarization and metastasis of esophageal squamous cell carcinoma via FAK/STAT3 pathway. *J Exp Clin Cancer Res* 2022;**41**:145.
46. Lui Y, Davis SJ. LAG-3: a very singular immune checkpoint. *Nat Immunol* 2018;**19**:1278–9.
47. Tao H, Cheng L, Liu L, Wang H, Jiang Z, Qiang X, et al. A PD-1 peptide antagonist exhibits potent anti-tumor and immune regulatory activity. *Cancer Lett* 2020;**493**:91–101.
48. Maruhashi T, Sugiura D, Okazaki IM, Shimizu K, Maeda TK, Ikubo J, et al. Binding of LAG-3 to stable peptide-MHC class II limits T cell function and suppresses autoimmunity and anti-cancer immunity. *Immunity* 2022;**55**:912–24.
49. Dileepan T, Malhotra D, Kotov DI, Kolawole EM, Krueger PD, Evavold BD, et al. MHC class II tetramers engineered for enhanced binding to CD4 improve detection of antigen-specific T cells. *Nat Biotechnol* 2021;**39**:943–8.
50. Tawbi HA, Schadendorf D, Lipson EJ, Ascierto PA, Matamala L, Castillo Gutiérrez E, et al. Relatlimab and nivolumab versus nivolumab in untreated advanced melanoma. *N Engl J Med* 2022;**386**:24–34.
51. Schöffski P, Tan DSW, Martín M, Ochoa-de-Olza M, Sarantopoulos J, Carvajal RD, et al. Phase I/II study of the LAG-3 inhibitor ieramilimab (LAG525) \pm anti-PD-1 spartalizumab (PDR001) in patients with advanced malignancies. *J Immunother Cancer* 2022;**10**:003776.
52. Zettl M, Wurm M, Schaaf O, Mostböck S, Tirapu I, Apfler I, et al. Combination of two novel blocking antibodies, anti-PD-1 antibody ezabenlimab (BI 754091) and anti-LAG-3 antibody BI 754111, leads to increased immune cell responses. *Oncol Immunology* 2022;**11**:2080328.
53. Thudium K, Selby M, Zorn JA, Rak G, Wang XT, Bunch RT, et al. Preclinical characterization of relatlimab, a human LAG-3-blocking antibody, alone or in combination with nivolumab. *Cancer Immunol Res* 2022;**10**:1175–89.
54. Maruhashi T, Sugiura D, Okazaki IM, Okazaki T. LAG-3: from molecular functions to clinical applications. *J Immunother Cancer* 2020;**8**:001014.
55. Robert C. LAG-3 and PD-1 blockade raises the bar for melanoma. *Nat Can (Ott)* 2021;**2**:1251–3.
56. Zhang Z, Liu X, Chen D, Yu J. Radiotherapy combined with immunotherapy: the dawn of cancer treatment. *Signal Transduct Targeted Ther* 2022;**7**:258.
57. Shang S, Liu J, Verma V, Wu M, Welsh J, Yu J, et al. Combined treatment of non-small cell lung cancer using radiotherapy and immunotherapy: challenges and updates. *Cancer Commun* 2021;**41**:1086–99.
58. Huang CT, Workman CJ, Flies D, Pan X, Marson AL, Zhou G, et al. Role of LAG-3 in regulatory T cells. *Immunity* 2004;**21**:503–13.
59. Muroyama Y, Nirschl TR, Kochel CM, Lopez-Bujanda Z, Theodoros D, Mao W, et al. Stereotactic radiotherapy increases functionally suppressive regulatory T cells in the tumor microenvironment. *Cancer Immunol Res* 2017;**5**:992–1004.